ChemComm

COMMUNICATION

View Article Online
View Journal | View Issue

Cite this: *Chem. Commun.*, 2023, **59**, 10012

Received 4th May 2023,
Accepted 12th July 2023

DOI: 10.1039/d3cc02175k

rsc.li/chemcomm

Graphene oxide-fullerene nanocomposite laminates for efficient hydrogen purification†

Qi Guo,[a] Behnam Ghalei,*[ab] Detao Qin,[ab] Daizu Mizutani,[a] Ikumi Joko,[ab] Habib Al-Aziz,[ab] Tomohiro Higashino,[a] Masateru M Ito,[ab] Hiroshi Imahori*[abc] and Easan Sivaniah*[ab]

Graphene oxide (GO) with its unique two-dimensional structure offers an emerging platform for designing advanced gas separation membranes that allow for highly selective transport of hydrogen molecules. Nevertheless, further tuning of the interlayer spacing of GO laminates and its effect on membrane separation efficiency remains to be explored. Here, positively charged fullerene C_{60} derivatives are electrostatically bonded to the surface of GO sheets in order to manipulate the interlayer spacing between GO nanolaminates. The as-prepared GO-C_{60} membranes have a high H_2 permeance of 3370 GPU (gas permeance units) and an H_2/CO_2 selectivity of 59. The gas separation selectivity is almost twice that of flat GO membranes because of the role of fullerene.

The growing demand for energy and global climate change caused by fossil fuel combustion threaten human survival. Hydrogen has been proposed as a clean, renewable energy source.[1] Currently, most hydrogen is produced *via* steam reforming and gasification of fossil fuels.[2] However, the resultant product, gray hydrogen, contains only ~50% hydrogen. Thus, it is necessary to remove CO_2 as a primary byproduct to achieve the hydrogen purity required by applications such as fuel cells.

Despite being a well-established method for removing CO_2 from H_2, chemical absorption can be energy-intensive and have several adverse environmental effects. On the other hand, membrane-based gas separation has emerged as a promising technology because of its simplicity to use, high energy efficiency, environmental friendliness, small footprint, and capability of continuous operation.[3] Polymeric membranes dominated the membrane industry due to their low cost and ability to withstand high-pressure gas feeds.[4] Nevertheless, most polymeric membranes suffer from low H_2 separation efficiency and a substantial trade-off between membrane selectivity and permeability, limiting their further development in designing high-performance membranes for H_2 purification.[5]

Recently, nanoporous materials such as zeolites,[6–8] metal–organic frameworks,[9,10] and carbon-based materials,[11,12] have attracted significant attention as alternative membrane materials. Graphene oxide (GO) nanolaminates are particularly interesting for H_2 purification due to their ability to form nanometric structures with superior H_2 sieving properties. GO nanolaminates were fabricated by a facile filtration method and showed high selectivity for H_2/CO_2 mixtures.[13] Theoretically, gases are separated by diffusing through selective gas transport channels in the GO membrane, composed of several interlayer spacing of GO nanosheets.

However, grain boundaries and random stacking of nanosheets lead to non-selective gas transport pathways in GO nanolaminates. The addition of nanomaterials, such as zeolitic imidazolate framework,[14–16] metal–organic framework,[17,18] hydroxy sodalite,[19] and organic polymer[20] to GO laminate may offer an opportunity to enhance the stacking of GO membranes, minimize non-selective pathways, and improve their separation performance. Nevertheless, the majority of composite nanolaminates reported to date contain nanofillers that are intrinsically incompatible with GO, restricting their uniform dispersion in GO matrixes.[21–24]

In order to find a highly compatible nanofiller for GO membranes, we examined other members of the carbon materials family, such as nanodiamonds. We have recently shown that incorporating positively charged nanodiamonds into GO nanolaminates significantly improved the humidity resistance of gas separation membranes.[25] However, incorporating of nanodiamonds with sp^3/sp^2 core/shell structure caused a slightly decreased gas selectivity compared to pure GO membranes. On the other hand, fullerene C_{60} and GO are both predominantly composed of sp^2 hybridized carbon atoms, making them intrinsically compatible. With its carbonaceous structure and

[a] *Department of Molecular Engineering, Graduate School of Engineering, Kyoto University, Kyoto, 615-8510, Japan. E-mail: imahori@scl.kyoto-u.ac.jp*
[b] *Institute for Integrated Cell-Material Sciences (iCeMS), Kyoto University, Kyoto, 606-8501, Japan. E-mail: bghalei@icems.kyoto-u.ac.jp, esivaniah@icems.kyoto-u.ac.jp*
[c] *Institute for Liberal Arts and Sciences (ILAS), Kyoto University, Kyoto, 606-8316, Japan*

† Electronic supplementary information (ESI) available. See DOI: https://doi.org/10.1039/d3cc02175k

nanometric size (~0.7 nm), C_{60} could act as a unique nanofiller to fine-tune the interlayer spacing and stacking behaviour of GO nanosheets. Furthermore, positively charged fullerene derivatives can be obtained through facile synthetic methods, which allows them to be combined orderly with negatively charged GO, using chemical bonds or electrostatic interactions.

In this study, we designed and synthesized three C_{60} derivatives with charge values of +1, +2, and +5 (Fig. S1, ESI†). The effects of C_{60} derivatives on the gas permeation and separation properties of GO-C_{60} nanocomposite membranes were investigated. Finally, we also discussed the impact of these positively charged C_{60} derivatives on GO nanolaminates' stacking, formation, and transport properties.

The materials and methods of this study are detailed in ESI.† The solubility of these derivatives in water increases as charge amounts and side groups increase, which is consistent with their UV-Vis absorbance. The zeta potentials of f1, f2, and f5 are 2, 18, and 34 mV, respectively. In the mixed solution of GO and f5, the zeta potential values decrease from −42 mV (GO) to −32 mV (GO + 20% f5) as f5 concentration increases (Fig. S2a–c, ESI†). This shows that the synthesized C_{60} derivatives can produce cations in an aqueous solution. Furthermore, C_{60} derivative cations are electrostatically bonded with negatively charged GO, resulting in a partial neutralization.

A single C_{60} derivative molecule is 1.1–1.6 nm in size based on theoretical calculations (GaussView, version 5.0.9). Dilute solutions (concentration: $1.65 \times 10^{-4} - 2 \times 10^{-3}$ mg mL^{-1}) of the C_{60} derivatives were used to make the membranes since they are prone to aggregate as concentration increases. Dynamic light scattering (DLS) and scanning electron microscope (SEM) show that the C_{60} nanoparticle clusters follow the order f1 > f2 > f5 in size (Fig. S2d and S3, ESI,† please note that the concentration to measure DLS and SEM is significantly higher than the concentration to make the membranes). f5 and f2 nanoparticle clusters show smaller sizes than that of f1 because of better solubility, higher charge density, and stronger electrostatic repulsion between particles.

According to the X-ray diffraction (XRD) pattern, the spacing between GO layers is 8.79 Å (Fig. S4 and Table S1, ESI†). Although this distance is larger than the kinetic diameters of both CO_2 (3.30 Å) and H_2 (2.89 Å) molecules, the stacked GO with sufficient thickness still provide a preference towards H_2 permeation over CO_2 because of the smaller size of H_2 molecules and stronger interaction between CO_2 and GO nanosheets. Thus, GO content plays a crucial role in determining separation performance as it adjusts the thickness of the resulting nanolaminates. The UV-visible absorption spectrum shows that GO aqueous solution has absorption within 400 nm. Since the absorbance varies linearly with concentration in the investigated range, the spectra can be used to determine GO mass in each membrane (Fig. S5, ESI†).

As a representative additive to GO laminates, we investigated the f5 loading effect on gas permeation and separation performances because it shows the highest solubility among the three C_{60} derivatives. The AAO support shows the H_2 permeance of 9107 GPU (gas permeance units, 1 GPU = 3.35×10^{-10} mol m^{-2} s^{-1} Pa^{-1}) with a low H_2/CO_2 selectivity of 8.5.

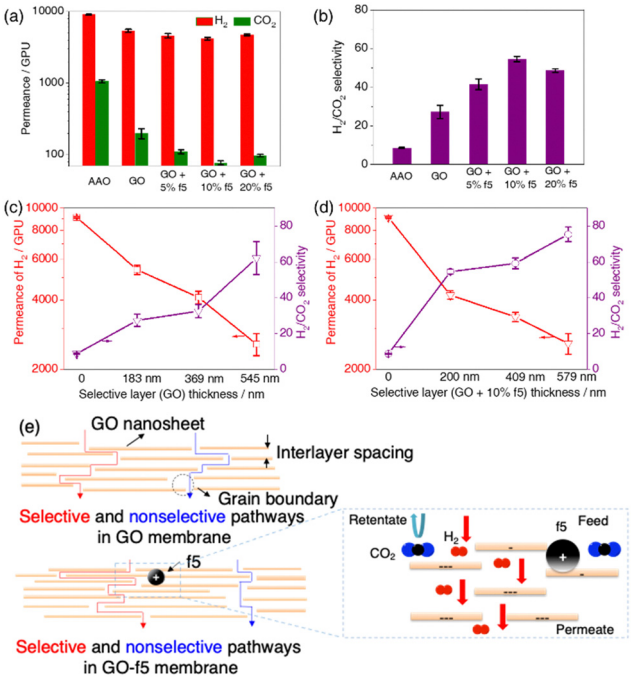

Fig. 1 H_2 and CO_2 permeance (a) and H_2/CO_2 selectivity (b) of GO-f5 membranes with different filler concentrations. H_2 permeance and H_2/CO_2 selectivity of GO membranes (c) and GO + 10% f5 membranes (d) with different thicknesses. (e) A schematic diagram for GO-C_{60} selective layer. Red and blue arrows represent the possible selective and non-selective gas pathways through each membrane, respectively. The black sphere with positive charge represents f5 particle.

The average H_2/CO_2 selectivity of GO membranes containing 0.1 mg GO increases to more than 27, indicating effective molecular sieving of GO laminates. As the f5 concentration in the GO-f5 series membrane rises from 0 to 20% (wt. all omitted below), H_2 and CO_2 permeance decreased gradually, whereas the H_2/CO_2 selectivity improved (Fig. 1a, b and Fig. S6, S7, ESI†). The membrane with 10% f5 has a slightly reduced permeance but has the highest selectivity, almost twice that of a pure GO membrane.

We further investigated the possibility of improving membrane gas selectivity by increasing membrane thickness. As GO membrane mass increases from 0.1 mg to 0.8 mg, gas permeance decreases and gas selectivity increases (Fig. 1c and Tables S2–S5, ESI†). A membrane containing 0.3 mg GO has the highest selectivity of 62, and the limited sensitivity of the instrument makes it impossible to detect permeated CO_2 in thicker samples. The gas permeance and selectivity of all membranes with GO and 10% f5 but different thickness shows similar trends with GO membranes, and the highest selectivity reaches 75 (Fig. 1d). Overall, membranes with f5 had higher selectivity than pure GO membranes of the same GO mass. As illustrated in Fig. 1e, the high density of negative functional groups on the edges of GO nanosheets enables the binding of f5 to GO, which reduces electrostatic repulsion between adjacent GO sheets. This results in narrower and more selective inter-gaps in GO-C_{60} nanolaminates than pure GO membranes. In other words, C_{60} derivative (f5) may prohibit

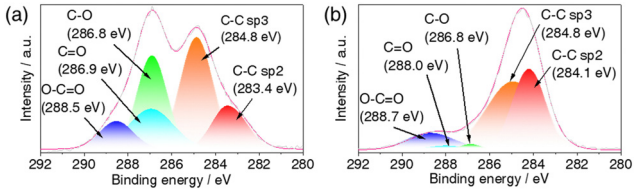

Fig. 2 XPS C 1s scanning spectra of (a) GO and (b) GO-f5 membranes.

CO_2 molecules from passing through the inter-grain boundaries of the GO membrane *via* electrostatic combination, while not for H_2 molecules. This hypothesis is supported by the X-ray photoelectron spectroscopy (XPS) data. As carboxylic groups are generally located on GO edges, the decrease in intensity of carboxylic peaks in the GO-f5 membrane over pure GO membrane confirms that carboxylic groups interact with f5 (Fig. 2). In addition, the XPS N 1s scanning spectra of f5 and the GO-f5 membrane show two N peaks of ammonium salt and amine, confirming the existence of f5 in the selective layer (Fig. S8, ESI†).

Fig. 3a and b show the SEM cross-sections of GO and GO-f5 membranes, respectively. Membranes containing 0.1, 0.2, and 0.3 mg GO have thicknesses of about 183, 369, and 545 nm, respectively, which is almost proportional to the mass of GO. The average thickness of membranes containing f5 was increased to about 200, 409, and 579 nm, respectively, compared with pure GO membranes with the same GO mass (Fig. S9, ESI†). The uniform increase in membrane thickness indicates the homogeneous incorporation of f5 particles into GO laminates as f5 concentration is $\leq$10%.

The SEM images of surface morphology are shown in Fig. 3c–f for the GO-f5 membrane samples with different f5 filler concentrations. The surface of a pure GO membrane is relatively smooth, whereas GO-f5 membranes have more rough surfaces. In low concentrations, *i.e.*, up to 10%, f5 fillers are associated with the inner GO sheets. However, at higher f5 concentrations, *i.e.*, 20 wt%, filler aggregation occurs on the surface of membranes, which makes non-selective voids in the laminate structure and lower separation efficiency than GO + 10% f5 membranes.

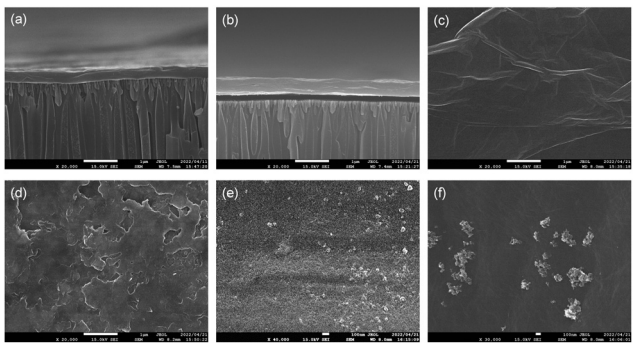

Fig. 3 Cross-section SEM images of (a) GO layer (0.2 mg) and (b) GO-f5 layer (GO 0.2 mg + 10% f5). Surface SEM images of (c) GO membrane (0.2 mg) and GO-f5 membranes (d: GO 0.2 mg + 5% f5; e: GO 0.2 mg + 10% f5; f: GO 0.2 mg + 20% f5).

XRD was used to confirm the interaction between GO and f5 and evaluate the crystal structure of the resulting membranes. The peaks around $2\theta = 9^\circ$–10° indicate the characteristic peak of GO (Fig. S4, ESI†). When f5 is added, the peak shifts to the left, indicating an increase in the average interlayer spacing of GO sheets. This is due to the fact that the size of inserted C_{60} derivative particles is substantially larger than the interspacing of the GO sheets. As the loading of f5 increases, the peak intensity gradually decreases, due to the reduced crystallinity of GO. The largest interlayer spacing (9.77 Å) is observed at 5% f5 concentration, indicating that f5 has been fully inserted into the GO interlayer. Further increasing the f5 loading amount will lead to f5 aggregation, which reduces the average interlayer spacing. XRD results also demonstrate that f5 tends to aggregate at higher concentrations, consistent with the SEM results.

Gas transport in GO-C_{60} nanolaminate membranes is influenced by two main types of porosities: nanoporous defects and interlayer spacings. Interlayer spacings offer high selectivity and act as molecular sieves, while nanoporous defects enhance permeance. However, the trend in H_2 permeance cannot be solely explained by changes in interlayer spacing. Initially, the introduction of C_{60} derivatives increases interlayer spacing, but its sealing properties significantly reduce gas transport through nanoporous pathways, leading to decreased H_2 permeance. Higher fullerene loading results in filler aggregation, reduced intercalation between GO nanosheets, and decreased interlayer spacing. Despite the decreased spacing, H_2 permeance increases due to the presence of nonselective defects caused by higher C_{60} loading.

We also developed composite membranes using other types of C_{60} derivatives, *i.e.* f1 and f2 as well as pristine fullerene ($C_{60,p}$). Membrane samples containing 0.2 mg GO and 10% f1 or f2 were tested using the same experimental procedure (Fig. 4a, see more discussions in ESI†).

The GO-C_{60} derivative membranes were assessed against other state-of-the-art H_2/CO_2 separation membranes (Fig. S10, S11 and Tables S6, S7, ESI†). Fig. 4b shows that the nanolaminate membranes developed in this study overcome the Robeson upper bound and have high permeance and selectivity.

In industrial production, separating H_2/N_2 and H_2/CH_4 is also in great demand. For example, the purge gas of ammonia production contains 60–70% H_2 and 20–25% N_2.[27] Also, the steam reforming of methane produces hydrogen-rich exhaust. Different from H_2/CO_2 separation, due to the low solubility of N_2 and CH_4 molecules, separating H_2 from these mixed gases through a conventional chemical absorption-based process is extremely difficult. Membrane technology has been an alternative strategy for H_2/N_2 and H_2/CH_4 separation. The ability of GO-f5 nanolaminate membrane for H_2/N_2 and H_2/CH_4 separation was also investigated. We chose the membrane with 0.2 mg GO and 10% f5 as a representative as it showed the best performance for separating H_2/CO_2. The membranes were tested using feed gases containing equal volumes of H_2/N_2 and H_2/CH_4. The results are shown in Fig. 4c, d and Tables S8, S9 (ESI†), which revealed that the GO-f5 membrane retains high H_2 selectivity. For H_2/N_2 and H_2/CH_4 separations, the selectivity

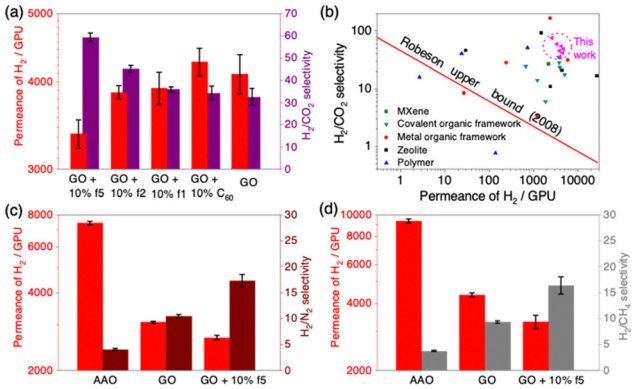

Fig. 4 (a) H_2 permeance and H_2/CO_2 selectivity of GO-C_{60} derivative membranes (GO: 0.2 mg; C_{60} derivatives: 10%). (b) H_2/CO_2 selectivity as a function of H_2 permeance for GO-C_{60} derivatives membranes in this work, compared with literature data (Fig. S10, ESI†).[6–10,26] H_2 permeance, H_2/N_2 selectivity (c) and H_2 permeance, H_2/CH_4 selectivity (d) of AAO support, GO, and GO + 10% f5 membranes.

was 17.2 and 16.3, respectively, which is a 65% and 77% improvement over pure GO membranes.

In summary, GO-C_{60} composite nanolaminates can efficiently separate hydrogen from gas mixtures. The optimum membrane structure achieved an H_2 permeance of 3370 GPU and an H_2/CO_2 selectivity of 59. The improvement in gas mixture selectivity derives from the introduction of f5, by tuning the interlayer spacing of GO laminates and sealing the grain boundary in GO sheets. The excellent compatibility and electrostatic interaction between positively charged C_{60} derivatives and negatively charged GO make f5 a good filler in GO gas separation membrane. The GO-C_{60} membrane herein is, to our knowledge, one of the best GO membranes for hydrogen separation. The high H_2 permeability and selectivity allow the GO-fullerene nanolaminate membrane to be an up-and-coming candidate for practical H_2 purification applications.

The authors acknowledge the funding under JSPS KIBAN-S KAKENHI (JP23H05468 (E. S.)), JSPS KIBAN-A KAKENHI (JP23H00309 (H. I.)), and JST-Mirai program (JPMJMI17E3 (E. S.)).

Conflicts of interest

There are no conflicts to declare.

Notes and references

1 A. Sartbaeva, V. L. Kuznetsov, S. A. Wells and P. P. Edwards, *Energy Environ. Sci.*, 2008, **1**, 79.
2 M. Voldsund, K. Jordal and R. Anantharaman, *Int. J. Hydrogen Energy*, 2016, **41**, 4969.
3 D. L. Gin and R. D. Noble, *Science*, 2011, **332**, 674.
4 A. G. Fane, R. Wang and M. X. Hu, *Angew. Chem., Int. Ed.*, 2015, **54**, 3368.
5 M. Ulbricht, *Polymer*, 2006, **47**, 2217.
6 X. Li, K. Li, S. Tao, H. Ma, R. Xu, B. Wang, P. Wang and Z. Tian, *Microporous Mesoporous Mater.*, 2016, **228**, 45.
7 Z. Hong, F. Sun, D. Chen, C. Zhang, X. Gu and N. Xu, *Int. J. Hydrogen Energy*, 2013, **38**, 8409.
8 K. P. Dey, D. Kundu, M. Chatterjee and M. K. Naskar, *J. Am. Ceram. Soc.*, 2013, **96**, 68.
9 F. Zhang, X. Zou, X. Gao, S. Fan, F. Sun, H. Ren and G. Zhu, *Adv. Funct. Mater.*, 2012, **22**, 3583.
10 N. Wang, A. Mundstock, Y. Liu, A. Huang and J. Caro, *Chem. Eng. Sci.*, 2015, **124**, 27.
11 H. Hatori, Y. Yamada, M. Shiraishi, H. Nakata and S. Yoshitomi, *Carbon*, 1992, **30**, 305.
12 D. Jiang, V. R. Cooper and S. Dai, *Nano Lett.*, 2009, **9**, 4019.
13 H. Li, Z. Song, X. Zhang, Y. Huang, S. Li, Y. Mao, H. J. Ploehn, Y. Bao and M. Yu, *Science*, 2013, **342**, 95.
14 X. Wang, C. Chi, J. Tao, Y. Peng, S. Ying, Y. Qian, J. Dong, Z. Hu, Y. Gu and D. Zhao, *Chem. Commun.*, 2016, **52**, 8087.
15 Y. Li, H. Liu, H. Wang, J. Qiu and X. Zhang, *Chem. Sci.*, 2018, **9**, 4132.
16 W. Li, J. Shi, Z. Li, W. Wu, Y. Xia, Y. Yu and G. Zhang, *Adv. Mater. Interfaces*, 2018, **5**, 1800032.
17 F. Yang, M. Wu, Y. Wang, S. Ashtiani and H. Jiang, *ACS Appl. Mater. Interfaces*, 2019, **11**, 990.
18 M. Jia, Y. Feng, S. Liu, J. Qiu and J. Yao, *J. Membr. Sci.*, 2017, **539**, 172.
19 H. Guo, G. Kong, G. Yang, J. Pang, Z. Kang, S. Feng, L. Zhao, L. Fan, L. Zhu, A. Vicente, P. Peng, Z. Yan, D. Sun and S. Mintova, *Angew. Chem., Int. Ed.*, 2020, **59**, 6284.
20 J. Shen, G. Liu, K. Huang, Z. Chu, W. Jin and N. Xu, *ACS Nano*, 2016, **10**, 3398.
21 S. Mohsenpour, A. W. Ameen, S. Leaper, C. Skuse, F. Almansour, P. M. Budd and P. Gorgojo, *Sep. Purif. Technol.*, 2022, **298**, 121447.
22 T. Wang, C. Cheng, L. Wu, J. Shen, B. V. Bruggen, Q. Chen, D. Chen and C. Dong, *Environ. Sci. Technol.*, 2017, **51**, 6202.
23 X. Zhu, C. Tian, C. Do-Thanh and S. Dai, *ChemSusChem*, 2017, **10**, 3304.
24 P. Guo-Wang, J. Ding, W. Guo, H. Wu, J. Wei, Y. Dai and F. Deng, *RSC Adv.*, 2016, **6**, 5688.
25 G. Huang, B. Ghalei, A. P. Isfahani, H. E. Karahan, D. Terada, D. Qin, C. Li, M. Tsujimoto, D. Yamaguchi, K. Sugimoto, R. Igarashi, B. K. Chang, T. Li, M. Shirakawa and E. Sivaniah, *Nat. Energy*, 2021, **6**, 1176.
26 (*a*) J. K. Das, N. Das and S. Bandyopadhyay, *J. Mater. Chem. A*, 2013, **1**, 4966; (*b*) J. K. Das and N. Das, *ACS Appl. Mater. Interfaces*, 2014, **6**, 20717; (*c*) K. Huang, Z. Dong, Q. Li and W. Jin, *Chem. Commun.*, 2013, **49**, 10326; (*d*) Y. Peng, Y. Li, Y. Ban and W. Yang, *Angew. Chem., Int. Ed.*, 2017, **56**, 9757; (*e*) M. Shan, X. Liu, X. Wang, I. Yarulina, B. Seoane, F. Kapteijn and J. Gascon, *Sci. Adv.*, 2018, **4**, eaau169; (*f*) H. Fan, A. Mundstock, A. Feldhoff, A. Knebel, J. Gu, H. Meng and J. Caro, *J. Am. Chem. Soc.*, 2018, **140**, 10094; (*g*) Y. Ying, D. Liu, J. Ma, M. Tong, W. Zhang, H. Huang, Q. Yang and C. Zhong, *J. Mater. Chem. A*, 2016, **4**, 13444; (*h*) B. Ghalei, Y. Kinoshita, K. Wakimoto, K. Sakurai, S. Mathew, Y. Yue, H. Kusuda, H. Imahori and E. Sivaniah, *J. Mater. Chem. A*, 2017, **5**, 4686; (*i*) L. Zhu, M. T. Swihart and H. Lin, *Energy Environ. Sci.*, 2018, **11**, 94; (*j*) S. H. Han, H. J. Kwon, K. Y. Kim, J. G. Seong, C. H. Park, S. Kim, C. M. Doherty, A. W. Thornton, A. J. Hill, A. E. Lozano, K. A. Berchtold and Y. M. Lee, *Phys. Chem. Chem. Phys.*, 2012, **14**, 4365; (*k*) Y. Li, H. Bux, A. Feldhoff, G. Li, W. Yang and J. Caro, *Adv. Mater.*, 2010, **22**, 3322; (*l*) H. Fan, M. Peng, I. Strauss, A. Mundstock, H. Meng and J. Caro, *Nat. Commun.*, 2021, **12**, 38; (*m*) R. Li, X. Fu, G. Liu, J. Li, G. Zhou, G. Liu and W. Jin, *J. Membr. Sci.*, 2022, **664**, 121097.
27 G. Yang, H. Guo, Z. Kang, L. Zhao, S. Feng, F. Jiao and S. Mintova, *ChemSusChem*, 2019, **12**, 4529.